A study of precipitates and insolubles in an Ni–Fe-based superalloy by analytical electron microscopy

R. Nakkalil
Department of Mechanical Engineering, The University of Manitoba, Winnipeg, Man. R3T 2N2 (Canada)
N. L. Richards
Bristol Aerospace Ltd., Winnipeg, Man. R3C 2S4 (Canada)
M. C. Chaturvedi
Department of Mechanical Engineering, The University of Manitoba, Winnipeg, Man. R3T 2N2 (Canada)

(Received December 24, 1991; in revised form March 2, 1992)

Abstract

This contribution discusses the results of an analytical electron microscopy study of precipitates and insolubles in the Ni–Fe-based superalloy Incoloy 903. The large insolubles in the alloy are observed to be carbides and/or carbonitrides of niobium and titanium. During thermomechanical processing, fine carbides are observed to precipitate on grain boundaries and prior grain boundaries. Also observed to precipitate along the grain boundaries and prior grain boundaries are MNP-type (M ≡ Nb, Ti; N ≡ Ni, Co, Fe) phosphides, a phase rich in niobium. The relative proportion of carbides to phosphides is observed to increase with an increase in the final solution treatment temperature, with complete phosphide dissolution at 975 °C/1 h. The phosphides are observed to have an orthorhombic crystal structure with cell dimensions $a = 5.99$ Å, $b = 3.35$ Å and $c = 7.06$ Å. The chemical composition of the coarse carbides, fine carbides and phosphides has been determined. The chemical composition and lattice parameter indicates the phosphides to be based on NbCoP with iron and nickel substituting for some of the cobalt sites.

1. Introduction

The 900 series superalloys represent a relatively new class of aerospace materials designed to provide high room and elevated temperature strength and a low coefficient of thermal expansion [1–3]. These alloys are based on the Fe–Ni–Co system with additions of niobium, aluminium and titanium for strengthening. In contrast to alternative high temperature superalloys, the chromium content is limited to optimize their low expansion characteristics. These alloys are precipitation hardenable and are primarily strengthened by $Ni_3(Al, Ti, Nb)$ γ' phase [1–3]. Currently, Incoloy 903 is the most widely used alloy of this family.

Optimum high temperature mechanical properties in alloy 903 are obtained by controlled thermomechanical processing and heat treatment. A typical treatment schedule involves warm working followed by a moderate anneal at 840 °C/1 h, which is below the recrystallization temperature and above the γ' solvus, and an aging treatment at 760 °C for 5 h followed by a furnace cool to 650 °C and further aging for 1 h. This processing sequence results in a highly textured microstructure and corresponding anisotropic mechanical properties. The duplex γ' particle size developed during precipitation hardening has been observed to give superior mechanical properties [4]. In principle, alloy 903 can be hot worked in the temperature range 815–1120 °C, but for superior stress rupture properties the final heat treatment temperatures should be a maximum of 925 °C with a minimum of 25% reduction at 870 °C or lower [1]. In addition to the phases that occur on aging, the presence of carbon in the 900 series alloys promotes the formation of niobium-rich cubic MX carbides and carbonitrides during ingot solidification and in the solid state during thermomechanical processing and heat treatment. Coarse niobium-rich MX carbides are present within the γ grains, typically aligned with the rolling direction. Cuboidal titanium-rich carbonitrides, often observed at the centre of the coarser carbides, serve as nucleation sites during ingot solidification. Depending on the thermomechanical processing and heat treatment, fine niobium-rich carbides may also form in the solid state at γ grain boundaries [2, 3].

The present study involves the microstructural

0921-5093/92/$5.00

characterization of the as-forged alloy 903 as well as alloys forged and solution treated at 840 °C/1 h, 925 °C/1 h, 950 °C/1 h and 975 °C/1 h. The microstructure prior to aging plays an important role in the age-hardening behaviour and the weldability of the alloy. The ultimate objective of the ongoing research is to relate the various microstructural variants to the weldability of alloy 903. This report presents the results of the characterization of insolubles and precipitates that form during the thermomechanical treatment and subsequent solution anneal before the hardening treatment using optical microscopy, X-ray diffraction, scanning electron microscopy–energy-dispersive spectrometry (SEM–EDS) and transmission electron microscopy–analytical electron microscopy (TEM–AEM).

2. Experimental details

An extruded billet of Incoloy 903 15.2 cm in diameter was thermomechanically processed by open die hammer forging to obtain the as-forged alloy. The billet was first forged to a 9.2 cm square cross-section from a temperature of 1121 °C by reductions of 1.3 cm in each step of forging. One intermediate reheat to 1121 °C was used during the process. The workpiece was then reheated to 927 °C and further forged in two equal steps to a 7.6 cm square cross-section with an intermediate reheat to 927 °C. The finishing temperature of the workpiece was about 816 °C. No further solution treatment was given to the material at this stage. Samples cut from this alloy are referred to as the "as-forged" specimens in all subsequent discussion. Some sections of the "as-forged" alloy were given solution treatments at 925 °C/1 h, 950 °C/1 h and 975 °C/1 h.

Another extruded billet of alloy 903 of length 11.4 cm and diameter 15.24 cm was soaked for 1 h at 1095 °C and upset forged, punched and sheared into a ring 6.4 cm thick of internal diameter 7.6 cm. The ring was then hot forged in five stages into a ring 4.6 cm thick of outer diameter 26.7 cm and internal diameter 19.4 cm. Preceding every stage, the temperature of the workpiece was raised to 840 °C by soaking it for a short time. In every stage of forging the ring was also hot rolled via rollers in a circumferential direction so as to obtain the requisite dimensions. The ring was given a solution treatment of 1 h at 840 °C following the final stage of processing. Since the material has primarily been forged, it is referred to as the "forged and solution-treated" ring in all subsequent discussion. The bulk chemical composition of the alloy in weight per cent (mill analysis) as obtained by the atomic absorption technique is given in Table 1.

The specimens of the alloy after various thermomechanical treatments—(a) "forged and solution-treated" ring, (b) "as-forged" billet, (c) "as-forged" billet solution treated at 925 °C/1 h, (d) "as-forged" billet solution treated at 950 °C/1 h and (e) "as-forged" billet solution treated at 975 °C/1 h—were investigated by optical microscopy, X-ray diffraction, SEM and TEM–AEM to ascertain the nature of grain size, insolubles and precipitate distribution. A Nikon optical microscope, a Jeol JXA 840 scanning X-ray microanalyser and a Jeol 2000 FX scanning transmission electron microscope were used for this purpose. Some samples of the "as-forged" alloy solution treated at 975 °C/1 h and further aged at 850 °C for 3 h were also studied to observe the precipitation behaviour.

X-ray diffraction studies were performed on bulk specimens as well as on the electrochemically extracted residue (extracted according to the ASTM E 963 schedule used for extraction of carbides, borides and topologically close packed phases in superalloys) using Cu Kα radiation with a nickel filter by diffractometry. The precise lattice parameter values were determined using the CELREF programme [5], which employs a least-squares refinement of the unit cell dimensions. SEM–EDS and SEM–backscattered electron (BSE) studies were undertaken to understand the nature and composition of the large insolubles. Carbon extraction replicas were prepared by standard techniques from all the samples and examined by TEM for morphological, crystal structure and microanalytical studies of the precipitates. The lattice parameters were determined from numerous reflections obtained from selected area diffraction (SAD) and microdiffraction patterns and refined with the CELREF programme. All the microanalyses were performed on EDS spectra obtained from thin precipitates on the carbon extraction replicas on either carbon-coated nylon grids or copper grids with the transmission electron microscope operating at 200 kV in a focused microprobe mode with a spot size of 40 nm. A double-tilt holder with zero-tilt readings was utilized. The acquisitions and analyses were

TABLE 1. Bulk alloy composition (wt.%)

Fe	Ni	Co	Nb	Ti	Al	Cr	Cu	Mn	Si	C	P	S	B
Balance	38.81	14.96	2.93	1.41	0.95	0.11	0.06	0.07	0.07	0.028	0.004	0.001	0.007

performed with a Tracor Northern high take-off angle Si(Li) detector coupled to a Tracor Northern model TN 5400 multichannel analyser. Semiquantitative analysis using theoretical Cliff–Lorimer k factors was utilized for the estimation of the chemical composition of the phases. However, care was taken to ensure that the X-ray acquisition came from only very thin areas and also only from precipitates not aligned along strongly diffracting orientations. At least 25 precipitates of each kind observed in the alloy were analysed to determine the average chemical composition.

3. Results and discussion

The microstructure of the as-received billet of Incoloy 903 prior to thermomechanical processing consisted of equiaxed grains with large insolubles randomly distributed in the material (Fig. 1(a)). The lattice parameter of the γ matrix as determined by X-ray diffraction on bulk samples is 3.602 Å. The insolubles were identified by X-ray diffraction as carbides and/or carbonitrides of MX type with an f.c.c. crystal structure and an average lattice parameter of 4.434 Å. The grain boundaries were observed to be devoid of any precipitation.

The microstructure of the as-forged alloy, forged and solution-treated ring and as-forged alloy solution treated at 925 °C/1 h consisted of a necklace structure (described below; Figs. 1(b) and 1(c)). The microstructure of the as-forged alloy solution treated at 950 °C consisted of a large amount of small, partially recrystallized grains with no clear-cut warm-worked grains (Fig. 1(d)), while the microstructure of the as-forged alloy solution treated at 975 °C consisted of fully recrystallized, equiaxed grains. A wide range of mixed grain structures, from fine recrystallized grains to coarse warm-worked grains, can be produced by careful control of the forging temperature, strain rate, total deformation and final solution treatment temperature [6]. The optimum balance of properties appears to be associated with the formation of the necklace structure, in which the material has only partially recrystallized [1–3, 6]. Recrystallized grains should, however, not be distributed randomly throughout the structure but should be in bands closely associated with the grain boundaries (Figs. 1(b) and 1(c)). Thus each warm-worked grain is surrounded by a

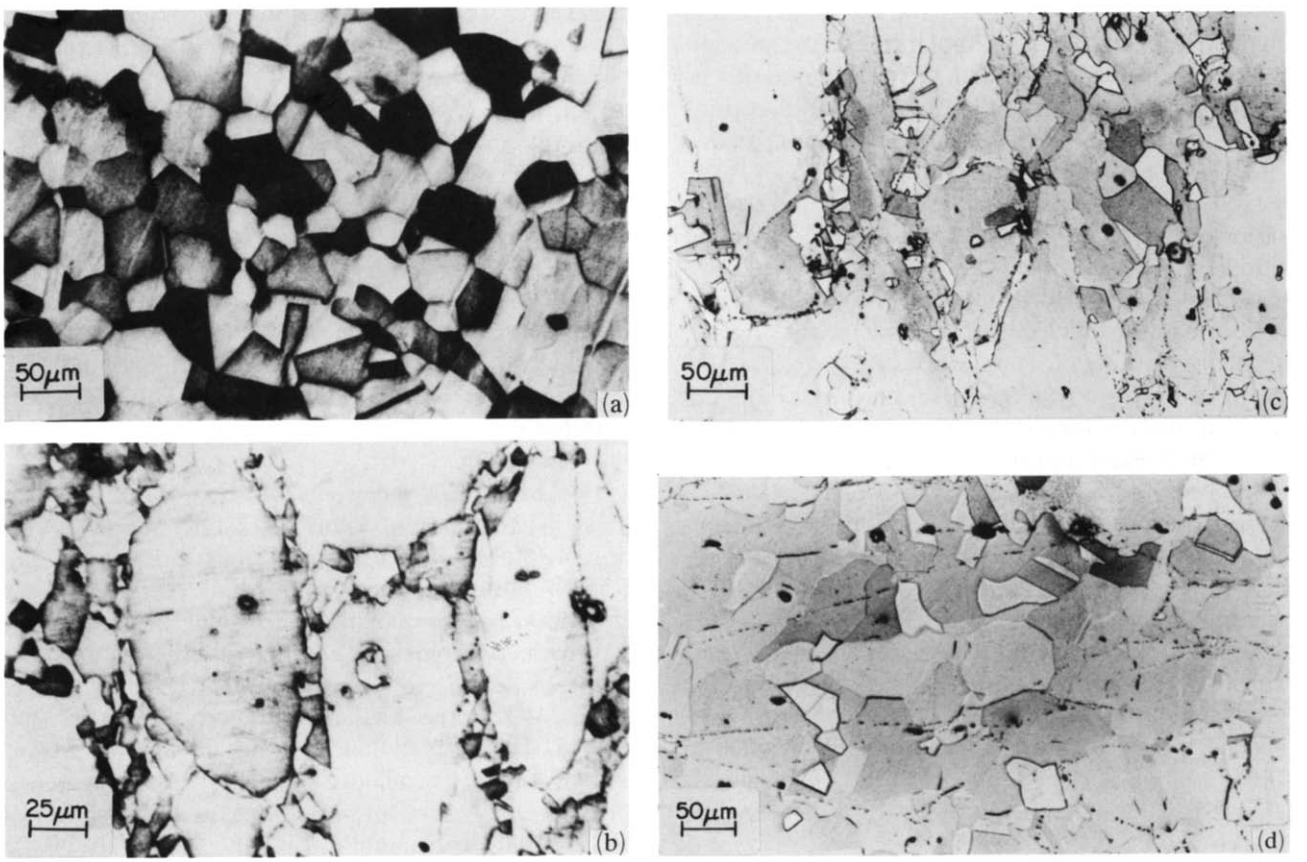

Fig. 1. Optical micrographs of (a) as-received extruded billet of alloy 903 prior to thermomechanical processing, (b) forged and solution treated ring, (c) as-forged alloy 903 solution treated at 925 °C/1 h and (d) as-forged alloy solution treated at 950 °C/1 h.

necklace of small recrystallized grains. It has also been reported [6] that for a good combination of fatigue and creep resistance the proportion of recrystallized to unrecrystallized grains should be within a certain range.

In Figs. 1(b)–1(d), large insolubles in the matrix, 5–10 μm in size and generally aligned in the rolling direction, and fine precipitates on the grain boundaries and prior grain boundaries can be observed. The thermomechanical processing the alloy has undergone is a multistep soaking, rolling and forging treatment. In this process some of the warm-worked grains formed in the preceding steps may be recrystallized. The annealed-out boundaries are outlined by fine precipitates. This feature is illustrated in Fig. 1(d), where the fine precipitates outline the annealed-out warm-worked grains. These boundaries are referred to as prior grain boundaries. As can be seen from the optical micrographs, the only difference between the two different forgings (the as-forged as well as various forged and solution-treated specimens *vs.* the forged and solution-treated ring) is the existence of precipitates on the prior grain boundaries in one set of forgings. In the case of the forged and solution-treated ring, all the precipitation during thermomechanical processing was confined to the existing boundaries (Fig. 1(b)). In the case of the as-forged alloy and alloys forged and solution treated at various temperatures, fine precipitates were observed on existing grain boundaries as well as on prior grain boundaries. Precipitates on prior grain boundaries in alloys forged and solution treated at 925 °C/1 h, 950 °C/1 h and 975 °C/1 h were observed possibly because of the increased recrystallization in these cases as compared to the forged and solution-treated ring. The difference between the as-forged alloy and the forged and solution-treated ring may be due to the allowable uncertainty in soaking and warm-working schedules in the industry.

X-ray diffraction studies were performed on the insolubles electrolytically extracted from the bulk material after the thermomechanical processing. The major constituent was observed to have an f.c.c. crystal structure with a lattice parameter of 4.434 Å. Minor peaks were also observed and were indexed as f.c.c. with a lattice parameter of 4.25 Å. Comparison of the data with the available literature [7–11] indicates the major component of the insolubles to be carbides and/or carbonitrides (MX type, f.c.c., X ≡ C, N, (C, N) and M ≡ Ti and/or Nb in the present case) based on titanium and niobium. The minor component appears to be TiN. It should be mentioned that very fine powder floated away during centrifuging and during the slide preparation for diffractometry.

Figure 2 shows an SEM–BSE image of a large insoluble. Two different phases in the insoluble—an outer region rich in higher atomic number elements than the matrix and an inner region (hereafter referred to as the nucleus) with lower atomic number elements than the matrix—can be identified. The chemical composition of these regions as determined by SEM–EDS quantitative microanalyses (Table 2) indicates the inner darker phase to be based on titanium and the larger outer phase to be based on niobium. We have no reliable evidence as to the proportion of carbon and nitrogen in any of the MX precipitates. The lattice parameters of the various carbides and carbonitrides based on niobium and titanium are too similar to one another [7–11] to allow any firm conclusion to be made based on the lattice parameter data. Hence, in further discussion, all of them are referred to as carbides. The metallic composition (Table 2) of the outer insoluble of the coarse carbides is 79.3 at.% Nb and 20.7 at.% Ti and that of the inner nucleus is 7.4 at.% Nb and 92.6 at.% Ti. These values conform well with previously reported data on carbides in similar families of superalloys [2, 3, 12].

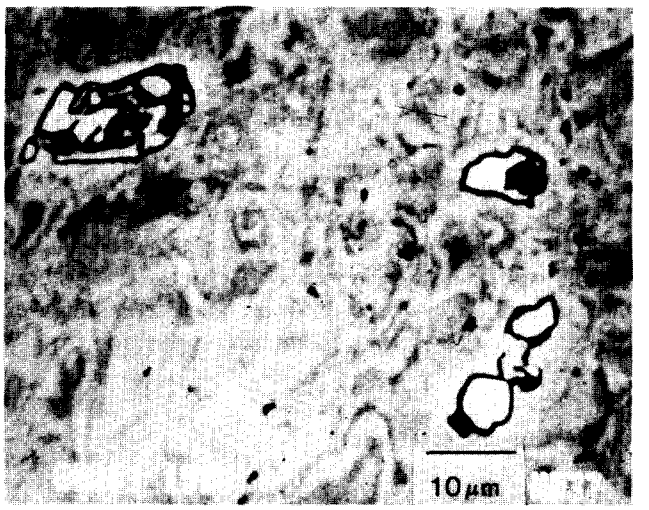

Fig. 2. SEM–BSE image of a large insoluble in the forged and solution-treated ring.

The SEM–EDS microanalyses confirm the existence of two different kinds of distinct phases in the large insoluble. Hence X-ray studies should yield two different lattice parameters. As discussed earlier, X-ray diffraction results on extracted insolubles did indicate two distinct carbides with lattice parameters of 4.434 and 4.25 Å. The reported values for the lattice parameters of TiN and TiC are 4.244 and 4.33 Å respectively [8]. Hence in conjunction with the microanalytical data it can be concluded that the inner nucleus is TiN–Ti(C, N). The preferred order of formation of MC carbides in superalloys is NbC and then TiC in order of decreasing stability [13]. This order is not the same as dictated by thermodynamics, which is TiC and

TABLE 2. Composition of insolubles and precipitates

1. Coarse carbides, MX type											
(a) Inner phase	Nb	Ti									
Average	7.4	92.6									
Maximum	9.3	95.6									
Minimum	4.4	90.7									
(b) Outer phase											
Average	79.3	20.7									
Maximum	84.1	24.0									
Minimum	76.0	15.9									
2. Fine carbides, MX type											
(a) Niobium rich	Nb	Ti									
Average	79.5	20.5									
Maximum	85.8	22.8									
Minimum	77.9	14.0									
(b) Titanium rich											
Average	57.8	42.2									
Maximum	67.6	57.1									
Minimum	39.2	32.4									
3. MNP-type phosphides											
(a) As forged	Nb	Ti	Fe	Co	Ni	P	Cr	Mo	Co:	Fe:	Ni
Average	44.5	2.5	13.0	16.1	11.7	11.7	—	—	0.39	0.32	0.29
Maximum	46.7	3.7	21.1	16.9	13.5	18.3	—	—			
Minimum	41.6	1.8	10.2	15.0	6.6	10.1	—	—			
(b) Forged and ST 975 °C											
Average	37.1	4.5	11.7	15.8	11.1	20.2	—	—	0.41	0.30	0.29
Maximum	40.3	7.6	16.8	22.4	15.8	24.9	—	—			
Minimum	30.1	2.9	9.7	13.3	9.2	11.6	—	—			
(c) Inconel 718 welds [8]	45.0	2.0	7.0	—	28.0	—	14.0	4.0			

Notes. (i) All compositions are given in atomic per cent. (ii) All compositions except for coarse carbides have been determined by STEM–EDS from particles on carbon extraction replicas. The data for coarse carbides have been obtained using SEM–EDS. (iii) All carbides found in alloy 903 were of MX type, where M refers to the metallic component (Nb, Ti in the present case) and X is C, N or (C, N). Only the metallic compositions are provided in the table. (iv) In MNP phosphides M refers to the 4d or 5d transition metal atoms (Nb, Mo, Ta, Zr, ...) and N refers to the 3d transition metal atoms (Fe, Co, Ni, Cr, ...). (v) See text for size, location and amount of various precipitates. (vi) ST, solution treated.

then NbC [13]. Carbides and nitrides are believed to form in superalloys before freezing [13]. During solidification, TiN–Ti(C, N) is the first phase to form from the melt. These particles serve as sites for the nucleation and growth of primary carbides from the melt. As discussed above, from kinetic considerations the formation of NbC is favoured over the formation of TiC. Hence NbC nucleates and grows around TiN–Ti(C, N). This yields the experimentally observed insoluble which has an inner nucleus comprising TiC and Ti(C, N) and an outer crust made up of niobium-rich carbide.

Figure 3 shows an SEM–BSE image of the as-forged alloy. Fine precipitates decorating grain boundaries and prior grain boundaries can be observed. Figure 4(a) shows a TEM bright field image of a carbon extraction replica of an as-forged specimen. Fine irregular precipitates along boundaries and prior grain boundaries can be observed. Figure 4(b) shows the

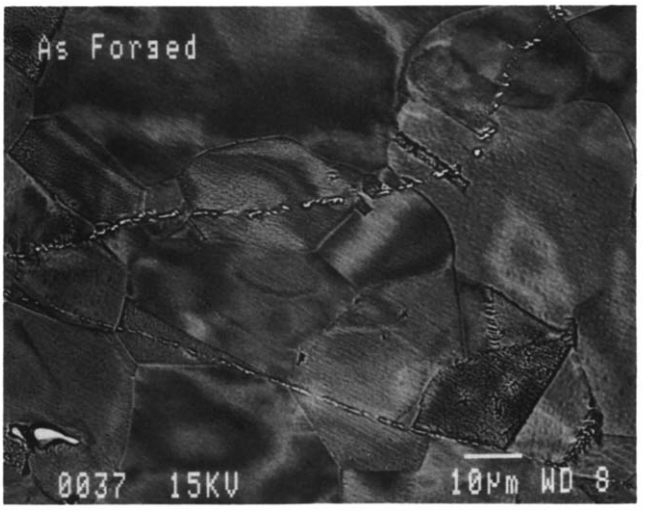

Fig. 3. SEM–BSE image showing fine precipitates on the grain boundaries and prior grain boundaries in an as-forged alloy.

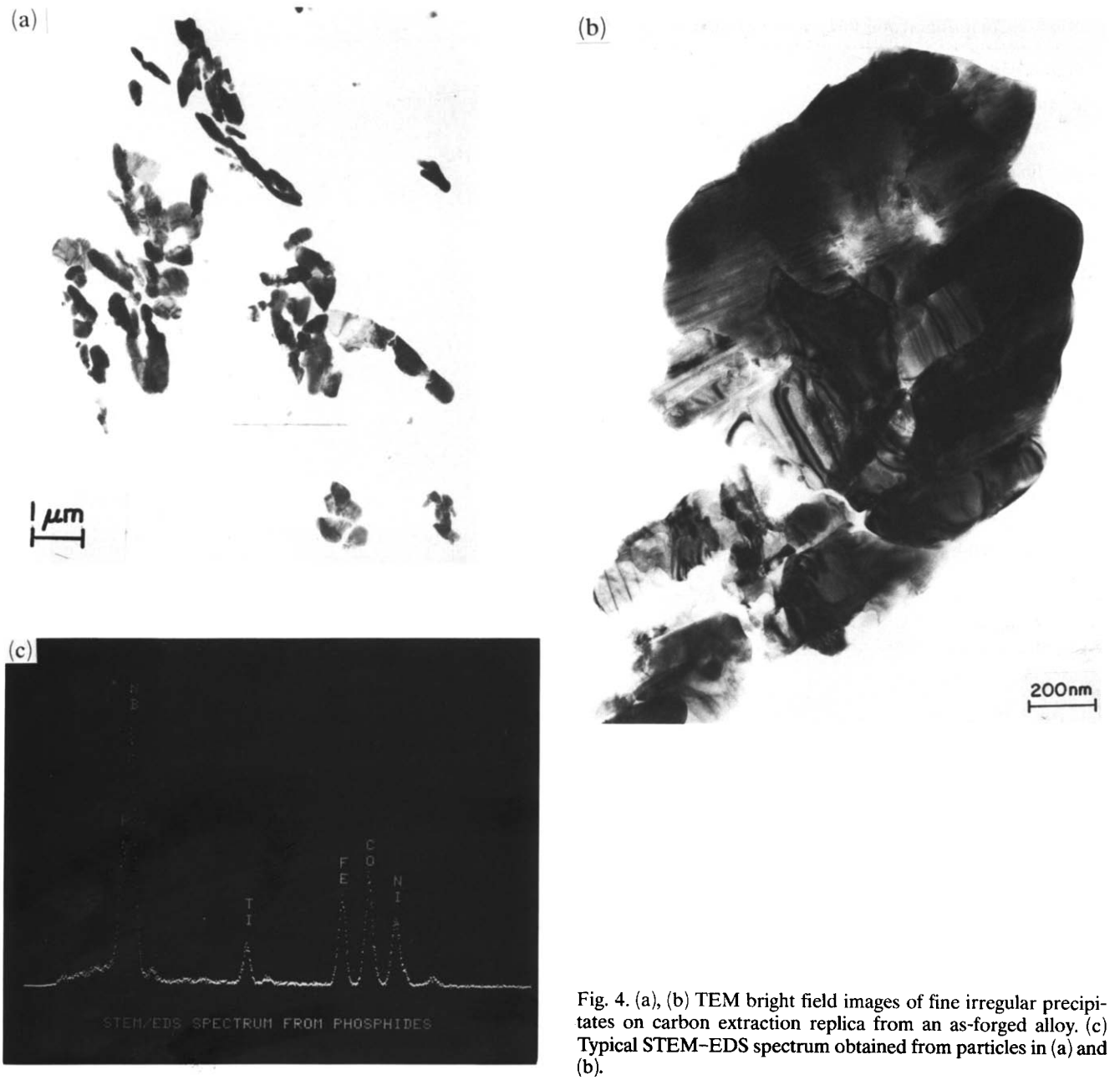

Fig. 4. (a), (b) TEM bright field images of fine irregular precipitates on carbon extraction replica from an as-forged alloy. (c) Typical STEM–EDS spectrum obtained from particles in (a) and (b).

microstructure of an individual particle. It can be seen that each particle is composed of fine misoriented crystallites with internal defects within them. Analysis of the various diffraction patterns indicates that they belong to an orthorhombic crystal structure with unit cell dimensions $a = 5.99$ Å, $b = 3.35$ Å and $c = 7.06$ Å. Figure 4 (c) shows an EDS spectrum obtained from one of these particles. A phosphorus Kα peak can be observed to the left of the niobium L multiplet. The chemical composition of the irregular precipitate particles observed in various samples as obtained from TEM–EDS X-ray microanalyses is given in Table 2. All the phases studied in the present investigation were observed to be non-stoichiometric. The chemical analysis presented is (1) the average value, (2) the maximum value and (3) the minimum value for each element in a given type of precipitate. Another kind of regular cuboidal particle was also observed on the boundaries and was found to be MX carbides (Tables 2 and 3, Figs. 5 and 6) by electron diffraction and microanalytical studies. For comparison, a TEM–EDS spectrum from a fine MX carbide found in the as-forged alloy solution treated at 975 °C/1 h is shown in Fig. 5. A pure niobium L multiplet can be observed.

The chemical analysis was performed using a standardless metallurgical thin film software package

TABLE 3. Crystallographic data on precipitates and insolubles

Precipitate	Technique	Space group	Unit cell dimensions (Å)
Coarse carbides	X-ray	*Fm3m*	*a* 4.434 (*v* = 87.2)
	X-ray		*a* 4.25 (76.8)
Fine carbides	SAD	*Fm3m*	*a* 4.43 (87)
[12]	SAD		*a* 4.42 (86.4)
[12]	SAD		*a* 4.25 (76.8)
MNP phosphides (NbCoP)	SAD	*Pnma*	*a* 5.99 *b* 3.35 (141.5) (0.848) *c* 7.06
NBNiP [12]	SAD		*a* 6.111 *b* 3.5 (151.64) (0.862) *c* 7.09
NbCoP [14, 15]	X-ray		*a* 6.112 *b* 3.587 (153) (0.876) *c* 6.978
NbNiP [14, 15]	X-ray		*a* 6.108 *b* 3.578 (155) (0.861) *c* 7.091
NbFeP [14]	X-ray		*a* 6.139 *b* 3.585 (154.2) (0.876) *c* 7.006

Note. The unit cell volume *v* (Å^3) is given in the first parentheses after the cell dimensions and the *a*/*c* ratio is provided in the next parentheses.

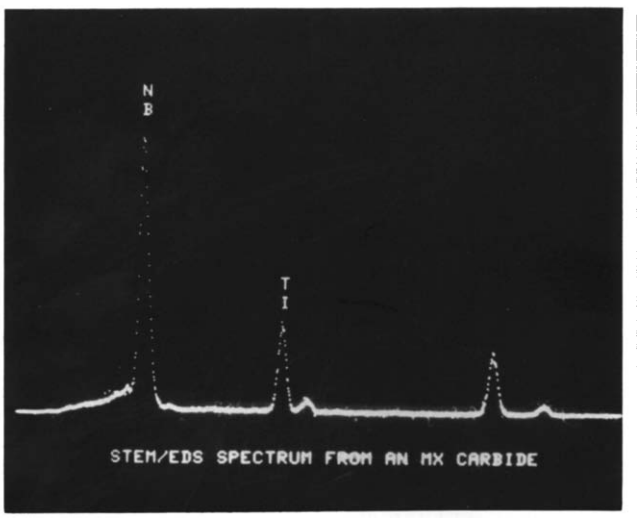

Fig. 5. Typical STEM–EDS spectrum obtained from a niobium-rich MX-type carbide.

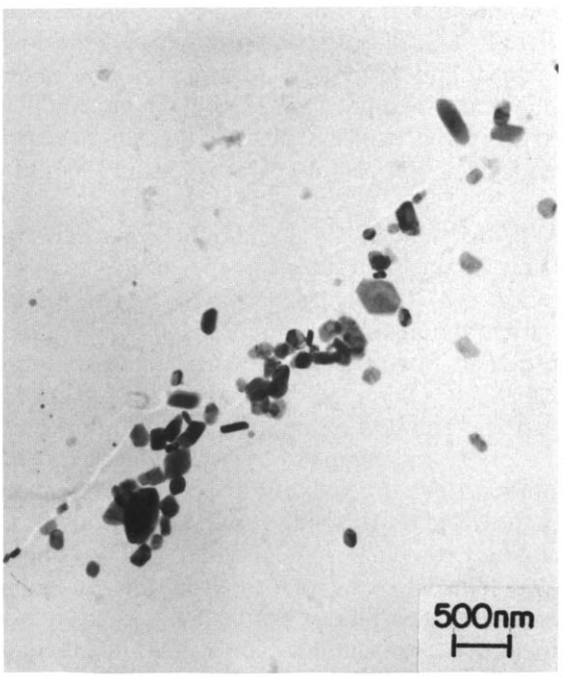

Fig. 6. TEM bright field image of fine carbides on carbon extraction replica from an as-forged alloy solution treated at 975 °C/1 h.

provided by Tracor Northern. The programme uses Kramer's law for background modelling but does not perform any deconvolution routine for assessment of the relative contribution of elements to overlapped peaks. However, since there is only a partial overlap between the niobium L multiplet and the phosphorus K doublet, the phosphorus compositions could be approximately assessed. Despite the uncertainty in the phosphorus and niobium composition analyses because of peak overlap, both are reported in Table 2 to give an indication of the composition values to a first approximation. The total possible error due to the semiquantitative analysis is assessed to be in the range

of 8%–13%. An alternative approach [12] would be to ignore the phosphorus counts in the spectra and perform the analyses. This amounts to normalizing the rest of the composition values. Both methods are prone to error, because in the latter approach the total niobium counts are overestimated by the number of buried phosphorus counts and the composition of the rest of the metallic elements is also overestimated because of the elimination of the phosphorus count. This approach [12] does not provide any idea of the phosphorus composition. The ideal solution would have been to perform deconvolution of the overlapped peaks, but in the absence of this technique it was felt that reporting the phosphorus composition would be helpful in fully appreciating the non-stoichiometric nature of the phase under investigation. The appreciable differences in the composition data in Table 2 are significant.

Comparison of the crystal structure and the composition data from the irregular precipitates with available literature data [14, 15] indicates them to belong to an MNP-type (M ≡ Nb, Ti; N ≡ Ni, Co, Fe) phosphide which to date has been reported only once in superalloys [12]. Vincent's data [12] on MNP-type phosphides observed in the heat-affected zone (HAZ) of alloy 718 weldments is given in Table 3 for comparison. Vincent [12] has reported only the composition analysis of the metallic elements in the phosphides and noted that the phosphorus composition appeared low for an equiatomic MNP-type phosphide. The main evidence for the existence of MNP-type phosphides stemmed from the crystal structure, the lattice parameter and the composition of the M- and N-type atoms.

Unlike Vincent [12], who found only 20 particles in one of the Inconel 718 weldments, in the present investigation MNP-type phosphides were found extensively in the as-forged alloy 903, the forged and solution-treated ring and the as-forged alloy solution treated at 925 °C. Some of the phosphides, except in the forged and solution-treated ring, were found outlining the prior grain boundaries, while in the forged and solution-treated ring, both phosphides and carbides were found only on the grain boundaries. The alloy solution treated at 975 °C/1 h had very few phosphides (less than 5% of the total particles, the rest being carbides). These phosphides were small and are likely to be the larger ones that have undergone insufficient dissolution. Their compositions have been analysed and reported separately in Table 2. In the forged and solution-treated ring, equal proportions of carbides and phosphides were observed, while in the as-forged alloy the proportion of phosphides to carbides was approximately 9:1.

As can be observed from Figs. 4(a) and 4(b), the size of the phosphides ranges from 0.1 to 0.5 μm. These are very easily recognizable on the extraction replicas owing to their irregular shape, small misoriented crystallites and the presence of internal defects. As stated, the only other particles observed on the replicas were fine MX-type carbides, which were easily differentiable owing to their distinct cuboidal shape (Fig. 6) with no internal defects. In some instances carbides were found to precipitate alongside the phosphides. It should be mentioned that in samples solution treated at 975 °C/1 h, traces of a randomly distributed non-stoichiometric phase rich in iron, chromium and aluminium were also observed. The uniqueness of the phosphide phases, their non-stoichiometric nature, their presence on the grain boundaries, their being stable only below 975 °C and their high niobium content entail a detailed discussion.

Many ternary equiatomic phosphides, MNP, are ordered versions of the Co_2P form of the anti-$PbCl_2$ structure. A large number of ternary silicides, germanides and phosphides crystallize with the Co_2P-type structure, which is a subclass of the anti-$PbCl_2$-type structure. The anti-$PbCl_2$ structure has two crystallographically non-equivalent metal positions, M and N. Compounds crystallizing with the anti-$PbCl_2$-type-structure can be divided into two subclasses with respect to their atomic coordination. Both subclasses belong to the space group *Pnma*. Typical representatives for the two subclasses are Co_2P and Co_2Si. The differences in coordination between the two subclasses are connected with the differences in the positional parameters of the atoms and also with an appreciable difference in the shape of the unit cells. It is also possible, barring borderline cases, to classify an anti-$PbCl_2$-type compound with respect to its type of coordination merely by determining its a/c ratio, which lies in the range 0.67–0.73 for the Co_2Si subclass and in the range 0.79–0.85 for the Co_2P subclass [14].

Atomic coordination values [15, 16] show that a structure of the Co_2P subclass would be particularly suited for ternary compounds containing two kinds of metal atoms with different radii, the larger metal atoms occupying the M positions with the highest coordination number and the smaller metal atoms occupying the N positions. The non-metal atoms have the coordination number nine, which is particularly common with phosphides and arsenides and frequently found in germanides. These compounds, also known as E phase [16, 17], contain 4d or 5d transition metal atoms as the larger atoms and 3d transition metal atoms as the smaller atoms. A number of MNP systems exist and Table 3 lists the ones relevant to the present investigation along with their unit cell dimensions. In analogy to *e.g.* the Laves phases, the abundance of E phases is likely due to the particularly favourable geometrical properties of the structure, allowing atoms

of different radii to be accommodated within a comparatively small unit cell [14, 18].

Rundqvist and Nawapong [14] have made an exploratory survey of M–N–P systems with Co_2P-type phases. Although they did not analyse the phase relationships in these systems in detail, they do report indications of extended homogeneity ranges of Co_2P-type phases in some of the systems. Deviations from ideal composition may occur through M–N substitution and through formation of vacancies in the lattice [14, 19]. Furthermore, the unit cell dimensions may exhibit variations even if the composition of the alloy is unchanged, depending on the degree to which M and N take ordered positions on the two non-equivalent metal atom sites in the structure [14]. Another interesting observation [20] for the Co_2P-type phases with the general formula MNX (M is a 4d or 5d transition metal, N is a 3d transition metal and X ≡ P, As, Si, Ge) is that compounds with cobalt as N type invariably have the smallest unit cell volume for any fixed combination of M and X components even though the normal metal radius for nickel is smaller than for cobalt. The major difference between NbCoP and NbNiP lies in the Co–Co and Ni–Ni distances. The latter distances exceed the former by more than three times the difference between any other pair of corresponding average distances.

Comparison of the present data shows that the closest approach to the composition and lattice constants of the phase under investigation is the NbCoP phase (Tables 2 and 3) with nickel and iron substituting for some of the N sites occupied by cobalt. The lattice parameter data agree within an error of 2% for *a*, less than 7% for *b* and less than 1% for *c* with NbCoP, within an error of 2% for *a*, less than 7% for *b* and less than 1% for *c* with NbNiP and within an error of less than 3% for *a*, less than 7% for *b* and less than 1% for *c* with NbFeP. It is not possible to identify any one of the above phases from the lattice parameter data alone, since the data agree within the same error with all three related compounds, NbCoP, NbNiP and NbFeP. However, the chemical composition provides some basis to make a conclusion. The chemical analysis obtained from the few, small, MNP-type phosphides observed in the specimen solution treated at 975 °C/ 1 h lends further credence to the fact that the observed phase is primarily based on NbCoP. The ratio of the amount of an element in the MNP-type phosphides to that in the matrix (*i.e.* *k*, the atomic percentage in the phosphide divided by the atomic percentage in the matrix) was observed to be 1.11 for cobalt and 0.31 for iron and nickel in the as-forged specimen, while in the specimen forged and solution treated at 975 °C the ratio was observed to be 1.09 for cobalt, 0.28 for iron and 0.29 for nickel. The occupancy ratio of N sites between cobalt, iron and nickel given in the last column of Table 2 also shows that cobalt is the most preferred of the three. The amount of metallic elements observed to be present in this study is consistent with equal proportions of M-type (Nb) and N-type (Co, Fe, Ni) atoms. These observations suggest that the phosphide observed in this investigation is based on NbCoP.

The composition of the non-metallic component, *i.e.* of phosphorus, appears low for an equiatomic MNP-type phosphide. Two possible causes for this behaviour are an extended homogeneity range and/or phosphorus–boron substitution in the phosphide. Unambiguous low phosphorus peaks were observed by Vincent [21] and in the present investigation on MNP-type phosphides. This could arise owing to the presence of an extended homogeneity range. This view is partly supported by the non-stoichiometric nature of the phosphides analysed in all the conditions of the alloy and by the observed decrease in niobium levels with a corresponding increase in phosphorus levels in the few phosphides observed in the as-forged alloy solution treated at 975 °C/1 h.

The metal-rich transition borides, silicides and phosphides are known to have many common crystal chemistry properties [22]. Studies by Rundqvist [22] show note-worthy phosphorus–boron substitution in binary phosphide structures. Jeitscho [23] showed that some metal-rich borides (MoCoB, WCoB and WFeB) crystallize with the anti-$PbCl_2$-type structure like the E phase. The NbCoB structure was shown [24] to be a combination of the anti-$PbCl_2$-type structure and the Fe_2P-type structure. NbFeB is isostructural with Fe_2P [25]. In all the above-mentioned cases, boron has been observed to have a coordination number of nine. Hence some of the non-metal sites in MNX-type structures can be occupied by boron without any changes in the crystal structure. Extending these observations to MNP phosphides found in the present investigation, it can be assumed that some boron substitution for phosphorus occurs. The unit cell volume is much smaller with boron substitutions. Some evidence for possible boron substitution is provided by the lower unit cell volume observed in this investigation as opposed to the values listed in the literature [14, 15]. It should, however, be pointed out that further confirmation is required through a detailed analysis of the phase relationships in the M–N–P systems of interest. Either similar studies on M–N–P–B systems or scanning transmission electron microscopy–electron energy loss spectroscopy (STEM–EELS) studies on the phosphides are required to ascertain if any boron is present in MNP phosphides observed in Incoloy 903.

As can be seen from Table 2, the cobalt, iron and nickel contents in the phosphides vary within a certain range from one precipitate to another owing to the

difference in the occupancy ratio of N-type metal atom sites between cobalt, iron and nickel. Depending on the relative amount of occupancy by iron, nickel and cobalt, slight changes in the unit cell dimensions may be expected, but the differences were too small to be detected by the SAD patterns. No change in the lattice parameter values was observed for phosphides in the samples with different heat treatments.

As the solution treatment temperature after the final thermomechanical treatment was increased, increased precipitation of fine carbides on the grain boundaries was observed. X-ray diffraction on bulk samples solution treated at 925 °C/1 h, 950 °C/1 h and 975 °C/1 h indicated increasing clarity and intensity of the MX reflections with an increase in the solution treatment temperature, confirming the precipitation of carbides. Figure 6 shows extensive carbide precipitation on the grain boundaries on a carbon extraction replica of an alloy treated for 1 h at 975 °C after forging. The size of the fine carbides in all the metallurgical conditions varies from 20 to 500 nm. They are found to be cuboidal in shape in all instances, with an f.c.c. crystal structure (point group $m3m$) and an average lattice parameter of 4.43 Å as obtained from the SAD patterns. The chemical composition obtained from TEM–EDS X-ray microanalyses on these particles on carbon extraction replicas is given in Table 2. All the carbides found in various conditions of alloy 903 are MX-type Hagg compounds with M sites occupied by niobium or titanium and X sites occupied by carbon, nitrogen or (C, N). No other carbide of any type was observed in any of the samples. Most of the carbides formed during precipitation were rich in niobium, the average niobium content being 79.5 at.% and the average titanium content being only 20.5 at.%. However, a few (trace) carbides were sometimes identified to be richer in titanium than niobium. These data can be seen from Table 2. Unlike the coarse carbides formed during ingot solidification, which have a distinct titanium-rich carbide as the nucleus around which the niobium-rich carbide grows, the carbides formed in precipitation during the thermomechanical processing rarely had such an inner nucleus and outer precipitate.

As mentioned earlier, we have no reliable evidence as to the proportion of carbon and nitrogen in any of the carbides. There have been numerous studies on carbides [7–11]. TiC has a lattice parameter of 4.33 Å and TiN a value of 4.244 Å [8]. The lattice parameter values of NbC range from 4.466 Å for NbC to 4.433 Å for $NbC_{0.72}$ [9]. While TiC and TiN are not completely soluble in each other [8], NbC and TiC are found in a continuous range of solid solution [10] with lattice parameters in the range 4.469–4.323 Å. $(Nb_{0.8}Ti_{0.2})C$ has a lattice parameter of 4.441 Å. Duwez and Odell [11] have examined the NbC–TiN and NbN–TiC systems and found continuous solid solutions. Because of these complications, it is not possible to attribute a unique composition to the carbides in alloy 903. The composition as well as the lattice parameter would vary in a certain range. However, all the nitrogen is expected to form nitrides and carbonitrides during solidification. Nitrides and carbonitrides have higher melting points and do not go into solution in any of the solution treatments. Hence it can be said with some certainty that the average fine carbides precipitating during heat treatments are of the type $(Nb_{0.8}Ti_{0.2})C$. The data on average lattice parameter (Table 3) and average metallic composition point towards this conclusion. The reason that the majority of the fine carbides are niobium rich is due to the fact the formation of NbC is kinetically favoured over TiC [13].

In order to examine whether MNP-type phosphides could be re-precipitated in the temperature range used for thermomechanical processing, some samples solution treated at 975 °C/1 h were aged for 3 h at 850 °C. Observations by TEM on carbon extraction replica from these samples confirmed extensive precipitation of MNP-type phosphides in clusters on grain boundaries. Figures 7(a) and 7(b) are TEM bright field images of MNP-type phosphides observed in these samples. The major difference between these precipitates and the ones found in thermomechanically processed material lies in the morphology. In the 850 °C/3 h aged samples it is not possible to generally distinguish the phosphides and the carbides except by composition analysis and electron diffraction. Both have similar size and morphology. These observations are similar to the observations of Vincent [12]. The MNP-type phosphides observed in the 850 °C aged samples did not contain any internal defects. These observations suggest that MNP-type phosphide particles are soft and become deformed during thermomechanical processing. The internal defects observed in the thermomechanically processed material are a direct consequence of the induced deformation. The carbides, however, are hard and remain undeformed during thermomechanical processing.

To our knowledge, there have been no TEM studies reported on Incoloy 903 in the open literature. Most of the prior work [2, 3] has been done using SEM–EDS on bulk samples. In the SEM–BSE mode the fine precipitates in Incoloy 903, irrespective of whether they are phosphides or carbides, appear brighter than the matrix owing to their higher niobium content. These precipitates are generally so fine that composition analysis by SEM gives only a higher niobium level with substantial nickel, iron and cobalt in all the cases because of the matrix interference. Hence no exact distinction can be made between the two phases, carbide and phosphide by SEM–EDS on bulk samples.

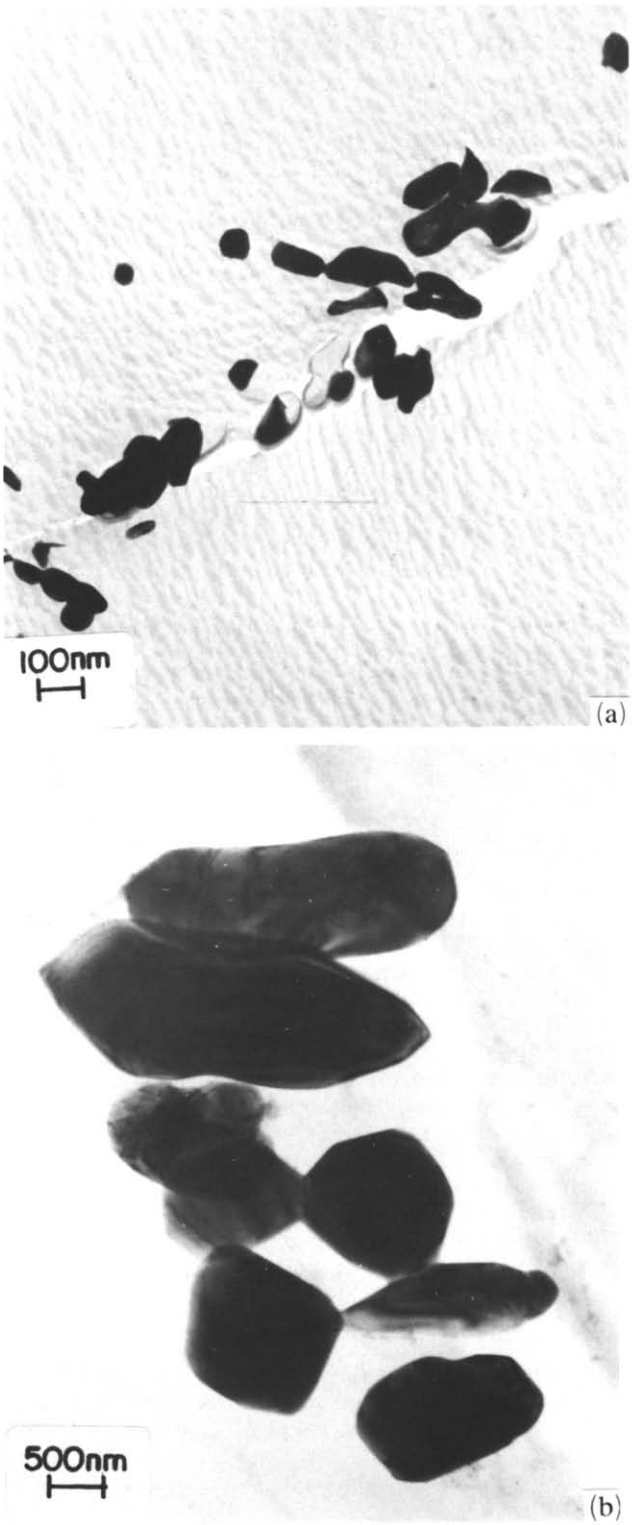

Fig. 7. TEM bright field images of re-precipitated MNP-type phosphides on carbon extraction replica from a forged alloy solution treated at 975 °C/1 h and aged for 3 h at 850 °C.

However, until now, owing to the higher niobium levels, the fine precipitates were always presumed to be MX-type carbides [2, 3]. The present AEM study conclusively shows that the fine precipitates can be either phosphides or carbides or a combination of both, depending on the temperatures used for the thermomechanical processing. This investigation shows that controlled thermomechanical processing is extremely important for obtaining the right combination of grain distribution and controlled precipitation.

MNP-type phosphides have not been hitherto observed in any of the superalloys except in the HAZ of an Inconel 718 weldment. The reason for their non-appearance in the other superalloys is twofold. Most of the superalloys are given solution treatments above 1000 °C. As observed in this study, the phosphides are not stable above 975 °C and hence no phosphides would be observed in the superalloys given final solution treatments in the range of 1000 °C and above. The second factor concerns the level of phosphorus in most of the superalloys. Phosphorus and sulphur are the main concerns of the residual non-metals in superalloys [26]. Extensive literature is available as to the detrimental affects of sulphur on various mechanical properties as well as on the weldability of the alloy, while there is a lack of literature as to the affect of phosphorus. There has been, however, one study on Inconel 600 [27] which clearly demonstrates that sulphur and phosphorus are extremely detrimental to weldability. Because of these reasons, the sulphur and phosphorus levels are generally kept low in the superalloys. Low temperature solution treatments are done for alloys 901, 903 and 907 because of the requirement of a necklace structure for optimum stress rupture properties. Hence, as can be seen from this investigation, there exists a possibility of phosphide precipitation.

Techniques for controlling the segregation of trace elements to grain boundaries are critically important for reliable mechanical, corrosion and welding performance in nickel-based superalloys [26]. In particular, elements such as phosphorus and sulphur are always deleterious, whereas boron (another melting point depressant [28]) may be deliberately added to the melt to improve the creep rupture properties by interaction with other grain boundary segregants [29]. Vincent's [12] results on Inconel 718 weldments point towards boron being the most likely segregant active as a melting point depressant, although the possible synergistic interactions with other trace elements could not be excluded. Kelly [30] also came to the same conclusion that boron is the single most detrimental element to the weldability of superalloys. The present investigation suggests segregation of phosphorus and possibly boron to the grain boundaries and their precipitation as MNX-type E phase. Liquation of this phase during welding leads to enrichment of niobium, phosphorus and boron concentration on the grain boundary. Enrichment of niobium [2, 3] and boron [12, 30] is observed to increase the microfissuring suscepti-

bility in the HAZ. The added presence of phosphorus along with niobium and boron is expected to exacerbate the HAZ microfissuring in Incoloy 903. Extensive HAZ microfissuring has been observed in electron beam welds of forged and solution-treated rings [31, 32].

4. Conclusions

The microstructure of forged Incoloy 903 has been investigated after various solution treatments.

(1) It has been observed that under the standard solution treatment time of 1 h, the necklace structure is preserved up to a solution treatment temperature of 925 °C.

(2) Niobium- and titanium-based coarse MX-type carbides formed during solidification were found to be aligned in the rolling direction. They have an inner nucleus rich in titanium, and an outer insoluble rich in niobium.

(3) During thermomechanical processing, fine carbides and phosphides are observed to precipitate along grain boundaries and prior grain boundaries.

(4) The phosphides are observed to be of equiatomic MNP type with niobium occupying the M sites and cobalt, iron and nickel occupying the N sites. They have an orthorhombic crystal structure (space group *pnma*) with lattice parameters $a = 5.99$ Å, $b = 3.35$ Å and $c = 7.06$ Å. The chemical composition of the phosphides has been determined. On the basis of the chemical composition and the lattice parameter, it is concluded that the phosphides are based on NbCoP with iron and nickel substituting partly for cobalt. Some boron substitution for phosphorus is also likely.

(5) If the final solution anneal is performed at 975 °C/1 h, extensive carbide precipitation and phosphide dissolution are observed. The kinetics of carbide precipitation is vastly enhanced by increasing the solution treatment temperature from 840 to 975 °C.

(6) The carbides have been observed to be of an MX type with an average lattice parameter of 4.43 A. The average chemical composition of the fine carbides has been determined by TEM-EDS.

(7) MNP-type phosphides have been observed to re-precipitate extensively on grain boundaries in the as-forged alloy solution treated at 975 °C/1 h and aged for 3 h at 850 °C.

Acknowledgments

Financial support for this work was provided by the National Science and Engineering Research Council of Canada through the University Industry Program, CRD Grant Ref. 661-009/88. R.N. also acknowledges a research fellowship from the Manitoba Hydro Corporation, Winnipeg, Manitoba.

References

1 Inco Alloys International Ltd., Incoloy 903, *Internal Rep.*, 1982.
2 W. A. Baeslack III, W. P. Lata, and S. L. West, *Weld. J., 67* (1988) 77-s.
3 C. Ernst, W. A. Baeslack III, and J. C. Lippold, *Weld. J., 68* (1989) 418-s.
4 E. Nembach, and G. Neite, *Prog. Mater. Sci., 29* (1985) 177.
5 D. E. Appleman, and H. T. Evans Jr., *Rep. USGS-GD-73-003*, 1973 (NITS, Springfield, VA).
6 P. J. Postans, and R. H. Jeal, *Proc. Forging and Properties of Aerospace Materials, Leeds, 1977*, Metals Society, London 1977, p. 300.
7 W. B. Pearson, *A Handbook of Lattice Spacings and Structures of Metals and Alloys*, Pergamon, Oxford, 1964.
8 D. W. Andrews, *J. Iron Steel Inst., 163* (1949) 384.
9 G. Brauer, H. Renner and J. Wernet, *Z. Anorg. Chem., 277* (1954) 249.
10 J. T. Norton, and A. L. Mowry, *J. Met., 1* (1949) 133.
11 P. Duwez, and F. Odell, *J. Electrochem. Soc., 97* (1950) 299.
12 R. Vincent, *Acta Metall., 33* (1985) 1205.
13 R. F. Decker, and C. T. Sims, in C. T. Sims and W. C. Hagel (eds.), *The Superalloys*, Wiley, New York, 1972, p. 54.
14 S. Rundqvist, and P. C. Nawapong, *Acta Chem. Scand., 20* (1966) 2250.
15 N. Chaichit, P. Chalugune, S. Rukvichai, P. Choosang, V. Kaewchansilp, C. Pontchour, P. Phavanantha and S. Pramatus, *Acta Chem. Scand. A, 32* (1978) 309.
16 J. H. Westbrook, R. K. Dicerbo and A. J. Peat, The nickel-titanium-silicon system, *General Electric Company, GE- 58 RL 2117*, 1958.
17 F. X. Spiegel, D. Bardos and P. A. Beck, *Trans. Metall. Soc. AIME, 227* (1963) 575.
18 C. B. Shoemaker, and D. P. Shoemaker, *Acta Crystallogr., 18* (1965) 900.
19 S. Rundqvist, *Acta Chem. Scand., 14* (1960) 1961.
20 S. Rundqvist and P. Tansuriwongs, *Acta Chem. Scand., 21* (1967) 813.
21 R. Vincent, in J. F. Mansfield (ed.), *Convergent Beam Diffraction of Alloy Phases*, Adam Hilger, Bristol, 1984, p. 76.
22 S. Rundqvist, *Acta Chem. Scand., 16* (1962) 1.
23 W. Jeitscho, *Acta Crystallogr. B, 24* (1968) 930.
24 P. I. Krypyakevich, Yu. B. Kuz'ma, Yu. V. Voroshilov, C. B. Shoemaker and D. P. Shoemaker, *Acta Crystallogr. B, 27* (1971) 257.
25 P. I. Krypyakevich, Ya. V. Markiv, and Ya. V. Melnyk, *Dopovidi Akad. Nauk Ukr. SSR, Ser. A*, (1967) 750.
26 R. T. Holt, and W. Wallace, *Int. Met. Rev., 21* (1976) 1.
27 W. F. Savage, E. Nippes, and G. M. Goodwin, *Weld. J., 56* (1977) 245-s.
28 J. L. Robinson, and M. H. Scott, *Philos. Trans. R. Soc. A, 295* (1980) 105.
29 E. Kny, W. Stolz, R. Stickler and H. Goretski, *J. Vac. Sci. Technol., 17* (1980) 1208.
30 T. Kelly, in S. A. David (ed.), *Advances in Welding Science and Technology*, ASM International, Metals Park, Ohio, 1986, p. 623.
31 R. Nakkalil, N. L. Richards, and M. C. Chaturvedi, *Scr. Metall. Mater., 26* (1992) 545.
32 R. Nakkalil, N. L. Richards, and M. C. Chaturvedi, *Trends in Welding Research III*, ASM, Metals Park, OH, 1992.